Numerical Solution of Steady-State Electromagnetic Scattering Problems Using the Time-Dependent Maxwell's Equations

ALLEN TAFLOVE AND MORRIS E. BRODWIN, SENIOR MEMBER, IEEE

***Abstract*—A numerical method is described for the solution of the electromagnetic fields within an arbitrary dielectric scatterer of the order of one wavelength in diameter. The method treats the irradiation of the scatterer as an initial value problem. At $t = 0$, a plane-wave source of frequency f is assumed to be turned on. The diffraction of waves from this source is modeled by repeatedly solving a finite-difference analog of the time-dependent Maxwell's equations. Time stepping is continued until sinusoidal steady-state field values are observed at all points within the scatterer. The envelope of the standing wave is taken as the steady-state scattered field. As an example of this method, the computed results for a dielectric cylinder scatterer are presented. An error of less than ±10 percent in locating and evaluating the standing-wave peaks within the cylinder is achieved for a program execution time of 1 min. The extension of this method to the solution of the fields within three-dimensional dielectric scatterers is outlined.**

I. INTRODUCTION

THE accurate determination of the electromagnetic fields within an arbitrary, inhomogeneous, dielectric scatterer is both an important theoretical problem and a practical objective of workers investigating the effects of microwaves upon living tissue. Exact analytical solutions are obtained only for simple scatterers like the sphere and the circular cylinder, which may be solved using separation of variables. For complicated scatterers like most body organs, we must resort to some numerical method if an accurate model is to be examined.

The computer techniques relevant to this problem that have appeared in the literature may be called, as a class, frequency-domain methods. These methods are based upon the assumption of an exp $(j2\pi ft)$ time dependence in the fundamental Maxwell's equations. In general, methods of this type derive a set of linear equations for either field variables or field expansion coefficients, and then solve the linear system with a suitable matrix-inversion scheme.

Wu and Tsai [1] solve two-dimensional scattering by an arbitrary dielectric cylinder. They develop a coupled integral equation pair for the electric field and its normal derivative at the surface of the scatterer. They then derive a corresponding set of linear equations for the surface fields using the moment method of Harrington [2]. Solution of this set of equations allows computation of the interior fields using Huygens' integrals. This method allows the very accurate solution of a homogeneous dielectric cylinder, about one free-space wavelength in circumference, by inverting an 80-by-80 matrix.

Manuscript received June 18, 1974; revised February 18, 1975.
The authors are with the Department of Electrical Engineering, Technological Institute, Northwestern University, Evanston, Ill. 60201.

McDonald and Wexler [3] solve a two-dimensional radiating antenna with dielectric obstacles. They employ a finite-element solution of the Helmholtz equation within a restricted region, and use an integral equation constraint along the contour of this region to take into account the unbounded exterior. Solution is obtained by inverting a 60-by-60 matrix.

Wilton and Mittra [4] solve two-dimensional scattering by an arbitrary dielectric cylinder. They expand the fields inside and outside of the scatterer in terms of free-space-type wave functions, wherever valid, and in terms of the analytic continuation of these wave functions, wherever required. The unknown set of coefficients is determined by enforcing the field boundary conditions at a number of points along the surface of the scatterer. Sufficient points are selected to represent the shape of the scatterer.

These three methods may be extended to more complicated scattering problems. Their accuracy is excellent when a sufficiently large set of linear equations is solved. However, each method may have two problems when very complicated inhomogeneous scatterers like body organs are considered. First, programming a complex scatterer requires the (possibly lengthy) derivation of a set of linear equations appropriate only for that scatterer. Second, solution of such a problem with high accuracy may require such a large, dense matrix to be inverted that the available fast, direct access computer storage is exhausted. As a comparison with the 80-by-80 matrix of Wu and Tsai, the maximum size dense matrix solvable using direct access storage, on the Northwestern University CDC 6400, is 400 by 400 [5].

The numerical method discussed in this paper is a time-domain approach, which treats the irradiation of the scatterer as an initial value problem. At $t = 0$, a plane-wave source of frequency f is assumed to be turned on. The propagation of waves from this source is simulated by solving a finite-difference analog of the time-dependent Maxwell's equations on a lattice of points, including the scatterer. Time stepping is continued until the sinusoidal steady state is achieved at each point. The field envelope, or maximum absolute value, during the final half-wave cycle of time stepping is taken as the magnitude of the phasor of the steady-state field.

This method has two advantages relative to frequency-domain approaches. First, and most important, it is simple to implement for complicated scatterers, because arbitrary dielectric parameters may be assigned to each lattice point. Second, its memory requirement is not prohibitive for many scatterers of interest. For example, the Northwestern computer can process a 125-by-250-point grid for two-dimensional problems, or a 20-by-20-by-40-point lattice for three-dimensional problems, without resorting to noncore storage. This is sufficient, using symmetry, to process a 12-wavelength-diam cylinder or a 2-wavelength-diam sphere.

This method has two disadvantages relative to frequency-domain approaches. First, its accuracy is only about ± 10 percent, which is at least one order of magnitude worse than that of the other methods. Second, the required program execution time may be excessive for some computer budgets. Typically, a two-dimensional problem solved on a 25-by-50-point grid, requires 1 min (at a rate of about 10 s/100 time steps). A three-dimensional problem solved on a 20-by-20-by-40-point lattice, requires 30 min (at a rate of about 5 min/100 time steps).

The important elements of the initial-value-problem approach to scattering problems are discussed below.

II. THE YEE ALGORITHM [6]

Using the MKS system of units, and assuming that the dielectric parameters μ, ϵ, and σ are independent of time, the following system of scalar equations is equivalent to Maxwell's equations in the rectangular coordinate system (x,y,z):

$$\frac{\partial H_x}{\partial t} = \frac{1}{\mu}\left(\frac{\partial E_y}{\partial z} - \frac{\partial E_z}{\partial y}\right) \tag{1a}$$

$$\frac{\partial H_y}{\partial t} = \frac{1}{\mu}\left(\frac{\partial E_z}{\partial x} - \frac{\partial E_x}{\partial z}\right) \tag{1b}$$

$$\frac{\partial H_z}{\partial t} = \frac{1}{\mu}\left(\frac{\partial E_x}{\partial y} - \frac{\partial E_y}{\partial x}\right) \tag{1c}$$

$$\frac{\partial E_x}{\partial t} = \frac{1}{\epsilon}\left(\frac{\partial H_z}{\partial y} - \frac{\partial H_y}{\partial z} - \sigma E_x\right) \tag{1d}$$

$$\frac{\partial E_y}{\partial t} = \frac{1}{\epsilon}\left(\frac{\partial H_x}{\partial z} - \frac{\partial H_z}{\partial x} - \sigma E_y\right) \tag{1e}$$

$$\frac{\partial E_z}{\partial t} = \frac{1}{\epsilon}\left(\frac{\partial H_y}{\partial x} - \frac{\partial H_x}{\partial y} - \sigma E_z\right). \tag{1f}$$

Yee introduces a set of finite-difference equations for the system of (1a)–(1f). Following Yee's notation, we denote a space lattice point as

$$(i,j,k) = (i\delta, j\delta, k\delta) \tag{2}$$

and any function of space and time as

$$F^n(i,j,k) = F(i\delta, j\delta, k\delta, n\delta t) \tag{3}$$

where $\delta = \delta x = \delta y = \delta z$ is the space increment, and δt is the time increment. Yee uses finite difference expressions for the space and time derivatives that are both simply programmed and second-order accurate in δ and in δt, respectively,

$$\frac{\partial F^n(i,j,k)}{\partial x} = \frac{F^n(i+\frac{1}{2},j,k) - F^n(i-\frac{1}{2},j,k)}{\delta} + 0(\delta^2) \tag{4}$$

$$\frac{\partial F^n(i,j,k)}{\partial t} = \frac{F^{n+1/2}(i,j,k) - F^{n-1/2}(i,j,k)}{\delta t} + 0(\delta t^2). \tag{5}$$

To achieve the accuracy of (4), and to realize all of the space derivatives of (1a)–(1f), Yee positions the components of $\bar{E}$ and $\bar{H}$ about a unit cell of the lattice as shown

in Fig. 1. To achieve the accuracy of (5), he evaluates $\bar{E}$ and $\bar{H}$ at alternate half-time steps. The result of these assumptions is the following system of finite-difference equations for the system of (1a)–(1f):

$$H_x^{n+1/2}(i,j+\tfrac{1}{2},k+\tfrac{1}{2}) = H_x^{n-1/2}(i,j+\tfrac{1}{2},k+\tfrac{1}{2}) + \frac{\delta t}{\mu(i,j+\tfrac{1}{2},k+\tfrac{1}{2})\delta} \cdot \left[\begin{array}{l} E_y^n(i,j+\tfrac{1}{2},k+1) - E_y^n(i,j+\tfrac{1}{2},k) + \\ E_z^n(i,j,k+\tfrac{1}{2}) - E_z^n(i,j+1,k+\tfrac{1}{2}) \end{array} \right] \quad (6a)$$

$$H_y^{n+1/2}(i+\tfrac{1}{2},j,k+\tfrac{1}{2}) = H_y^{n-1/2}(i+\tfrac{1}{2},j,k+\tfrac{1}{2}) + \frac{\delta t}{\mu(i+\tfrac{1}{2},j,k+\tfrac{1}{2})\delta} \cdot \left[\begin{array}{l} E_z^n(i+1,j,k+\tfrac{1}{2}) - E_z^n(i,j,k+\tfrac{1}{2}) + \\ E_x^n(i+\tfrac{1}{2},j,k) - E_x^n(i+\tfrac{1}{2},j,k+1) \end{array} \right] \quad (6b)$$

$$H_z^{n+1/2}(i+\tfrac{1}{2},j+\tfrac{1}{2},k) = H_z^{n-1/2}(i+\tfrac{1}{2},j+\tfrac{1}{2},k) + \frac{\delta t}{\mu(i+\tfrac{1}{2},j+\tfrac{1}{2},k)\delta} \cdot \left[\begin{array}{l} E_x^n(i+\tfrac{1}{2},j+1,k) - E_x^n(i+\tfrac{1}{2},j,k) + \\ E_y^n(i,j+\tfrac{1}{2},k) - E_y^n(i+1,j+\tfrac{1}{2},k) \end{array} \right] \quad (6c)$$

$$E_x^{n+1}(i+\tfrac{1}{2},j,k) = \left[1 - \frac{\sigma(i+\tfrac{1}{2},j,k)\delta t}{\epsilon(i+\tfrac{1}{2},j,k)}\right] E_x^n(i+\tfrac{1}{2},j,k) + \frac{\delta t}{\epsilon(i+\tfrac{1}{2},j,k)\delta} \cdot \left[\begin{array}{l} H_z^{n+1/2}(i+\tfrac{1}{2},j+\tfrac{1}{2},k) - H_z^{n+1/2}(i+\tfrac{1}{2},j-\tfrac{1}{2},k) + \\ H_y^{n+1/2}(i+\tfrac{1}{2},j,k-\tfrac{1}{2}) - H_y^{n+1/2}(i+\tfrac{1}{2},j,k+\tfrac{1}{2}) \end{array} \right] \quad (6d)$$

$$E_y^{n+1}(i,j+\tfrac{1}{2},k) = \left[1 - \frac{\sigma(i,j+\tfrac{1}{2},k)\delta t}{\epsilon(i,j+\tfrac{1}{2},k)}\right] E_y^n(i,j+\tfrac{1}{2},k) + \frac{\delta t}{\epsilon(i,j+\tfrac{1}{2},k)\delta} \cdot \left[\begin{array}{l} H_x^{n+1/2}(i,j+\tfrac{1}{2},k+\tfrac{1}{2}) - H_x^{n+1/2}(i,j+\tfrac{1}{2},k-\tfrac{1}{2}) + \\ H_z^{n+1/2}(i-\tfrac{1}{2},j+\tfrac{1}{2},k) - H_z^{n+1/2}(i+\tfrac{1}{2},j+\tfrac{1}{2},k) \end{array} \right] \quad (6e)$$

$$E_z^{n+1}(i,j,k+\tfrac{1}{2}) = \left[1 - \frac{\sigma(i,j,k+\tfrac{1}{2})\delta t}{\epsilon(i,j,k+\tfrac{1}{2})}\right] E_z^n(i,j,k+\tfrac{1}{2}) + \frac{\delta t}{\epsilon(i,j,k+\tfrac{1}{2})\delta} \cdot \left[\begin{array}{l} H_y^{n+1/2}(i+\tfrac{1}{2},j,k+\tfrac{1}{2}) - H_y^{n+1/2}(i-\tfrac{1}{2},j,k+\tfrac{1}{2}) + \\ H_x^{n+1/2}(i,j-\tfrac{1}{2},k+\tfrac{1}{2}) - H_x^{n+1/2}(i,j+\tfrac{1}{2},k+\tfrac{1}{2}) \end{array} \right]. \quad (6f)$$

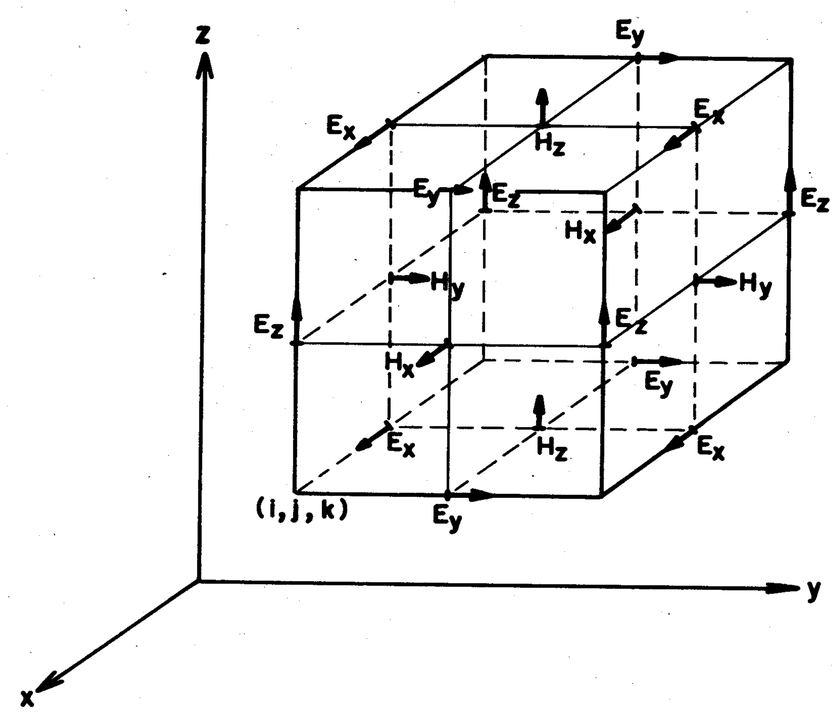

Fig. 1. Positions of the field components about a unit cell of the Yee lattice.

With the system of (6a)–(6f), the new value of a field vector component at any lattice point depends only on its previous value and on the previous values of the components of the other field vector at adjacent points. Therefore, at any given time step, the computation of a field vector may proceed one point at a time. Computer storage must be provided for 11 quantities at each unit cell of the lattice: the 6 field vector components, the values of ϵ and σ, and the maximum $|E_x|$, $|E_y|$, and $|E_z|$ achieved during the final half-wave cycle of time stepping.

The choice of δ and δt is motivated by the reasons of accuracy and stability, respectively. To ensure the accuracy of the computed results, δ must be taken as a small fraction of either the minimum wavelength expected in the model or the minimum scatterer dimension. Thus the field cannot change significantly over one space increment, and the cubic lattice approximation to the smooth scatterer surface cannot be too coarse. To ensure the stability of the time-stepping algorithm of (6a)–(6f), δt is chosen to satisfy

$$v_{max}\delta t \leq \left(\frac{1}{\delta x^2} + \frac{1}{\delta y^2} + \frac{1}{\delta z^2}\right)^{-1/2} \quad (7)$$

where v_{max} is the maximum wave phase velocity expected within the model. The corresponding stability criterion set forth by Yee in (7) and (8) of his paper is incorrect. The derivation of (7) is outlined in the Appendix.

III. THE LATTICE TRUNCATION CONDITIONS

A basic problem with any finite-difference solution of Maxwell's equations is the treatment of the field vector components at the lattice truncation. Because of limited computer storage, the lattice cannot cover a sufficiently large portion of space so that the scattered wave at the lattice truncation might be closely approximated. Necessarily, the lattice must terminate close to the scatterer in a region where the nature of the scattered wave is unknown.

Proper truncation of the lattice requires that any outgoing wave disappear at the lattice boundary without re-

flection during the continuous time stepping of the algorithm. Improper truncation results in error for all time steps after the boundary wave reflections return to the vicinity of the scatterer. This is exemplified by Yee's fixing of the field components at each truncation point at zero, for all time steps. This "hard" truncation condition does not take into account the values of the fields of any possible outgoing wave and causes boundary reflections in a way analogous to reflection at the surface of a conductor.

One way to achieve a "soft" lattice truncation is to assign linearly increasing values of σ near the lattice boundary so that absorption of outgoing waves is achieved. However, for a small value of reflection, the distance over which absorption takes place must be of the order of one wavelength. For many problems, this is an intolerable assignment of computer storage to points not in the scatterer. In addition, any incident wave propagating parallel to such a lattice boundary must suffer distortion due to the variation of phase velocity along the wavefront. Therefore, this type of truncation is not suitable.

A more desirable soft lattice truncation relates in a simple way the values of the field components at the truncation points to field component values at points one or more δ within the boundary. This is illustrated using the one-dimensional lattice of Fig. 2, for the time-step relation $c\delta t = \delta$

$$E_z^n(M) = E_z^{n-1}(M-1). \tag{8a}$$

Equation (8a) simulates the free-space propagation of the magnitude of E_z from the point $M-1$ to the truncation point M in one time step (the numerical propagation delay implied by the time-step relation). This is an exact truncation condition for the lattice of Fig. 2, in that all possible $+y$-directed waves are absorbed at M without reflection. If we wish to simulate the truncation of this lattice in an infinite dielectric half-space of refractive index m, (8a) is modified to

$$E_z^n(M) = E_z^{n-m}(M-1). \tag{8b}$$

Unfortunately, no simple, exact soft truncation condition analogous to (8a), (8b) is apparent for either the two- or three-dimensional space lattices. This is because any particular outgoing wave cannot be assumed to be plane and normally incident on one lattice boundary plane. At any truncation point, the local angle of incidence of this wave, relative to the boundary, is unknown. Further, several different waves having varying local angles of incidence may arrive at the same time. No simple, single truncation condition can account for all of these possibilities. Therefore, we can arrive at only an approximate truncation condition that reduces the effective lattice boundary reflection coefficient to an acceptable level.

An example of a set of simple, approximate, soft lattice truncation conditions is illustrated using the two-dimensional lattice of Fig. 3, for the time-step relation $c\delta t = \frac{1}{2}\delta$

$$E_z^n(i,0) = (E_z^{n-2}(i-1,1) + E_z^{n-2}(i,1) + E_z^{n-2}(i+1,1))/3 \tag{9a}$$

$$E_z^n(i,49) = (E_z^{n-2}(i-1,48) + E_z^{n-2}(i,48) + E_z^{n-2}(i+1,48))/3 \tag{9b}$$

$$H_y^n(\tfrac{1}{2},j) = (H_y^{n-2}(1\tfrac{1}{2},j-1) + H_y^{n-2}(1\tfrac{1}{2},j) + H_y^{n-2}(1\tfrac{1}{2},j+1))/3 \tag{9c}$$

$$H_y^n(50\tfrac{1}{2},j) = (H_y^{n-2}(49\tfrac{1}{2},j-1) + H_y^{n-2}(49\tfrac{1}{2},j) + H_y^{n-2}(49\tfrac{1}{2},j+1))/3. \tag{9d}$$

Equations (9a)–(9d) allow the field value at any lattice truncation point to rise to approach the field value of any outgoing wave, thus lowering the effective reflection coefficient at the boundary. This is done by simulating the propagation of an outgoing wave from the lattice plane adjacent to the truncation, to the lattice plane at the truncation, in a number of time steps corresponding to the propagation delay. The averaging process is used to take into account all possible local angles of incidence of the outgoing wave at the lattice boundary, and possible multiple incidences.

The effectiveness of (9a)–(9d) in reducing lattice boundary reflections is illustrated in Fig. 4, which plots the computed propagation of an outgoing cylindrical wave in the grid of Fig. 3. The outgoing wave is a Gaussian pulse originating from an excitation at grid point 25,24. The pulse is approximately 200 ps long, and has a maximum $|E_z| = 1000$. δ is set at 0.3 cm, and δt is set at 5 ps. In the figure, contours of constant E_z are superimposed on the left half of the grid (the right half is omitted because of symmetry) at intervals of 20 time steps. The pulse

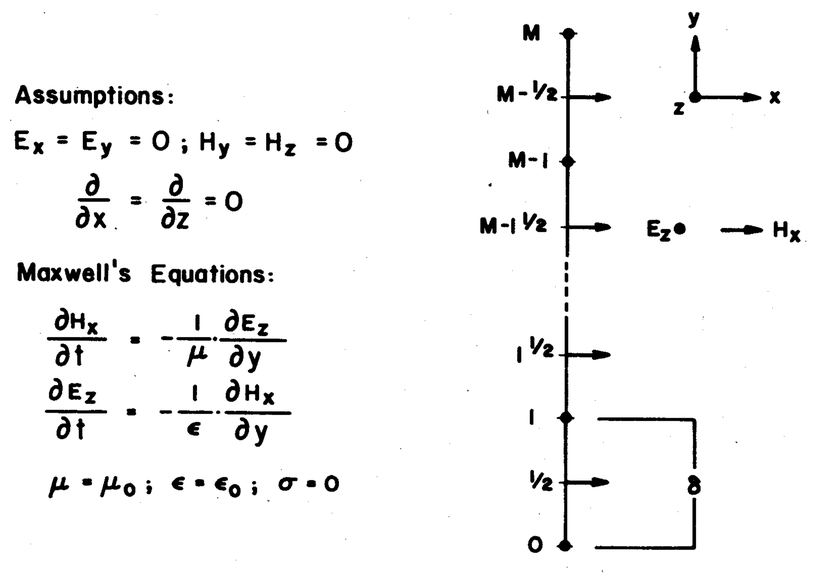

Fig. 2. One-dimensional lattice, illustrating a soft lattice truncation at M.

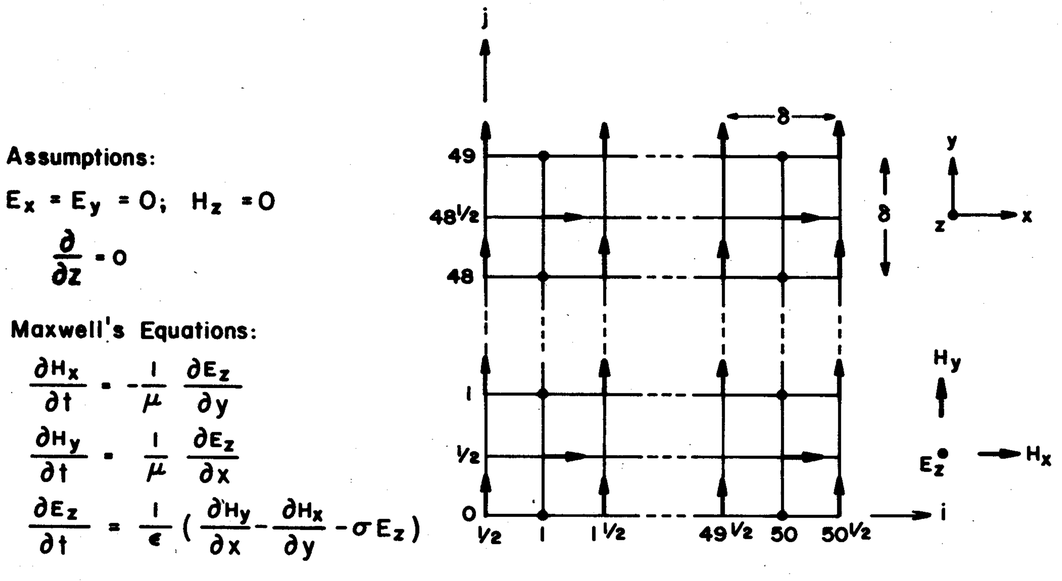

Fig. 3. Two-dimensional lattice, illustrating a set of approximate soft lattice truncation conditions.

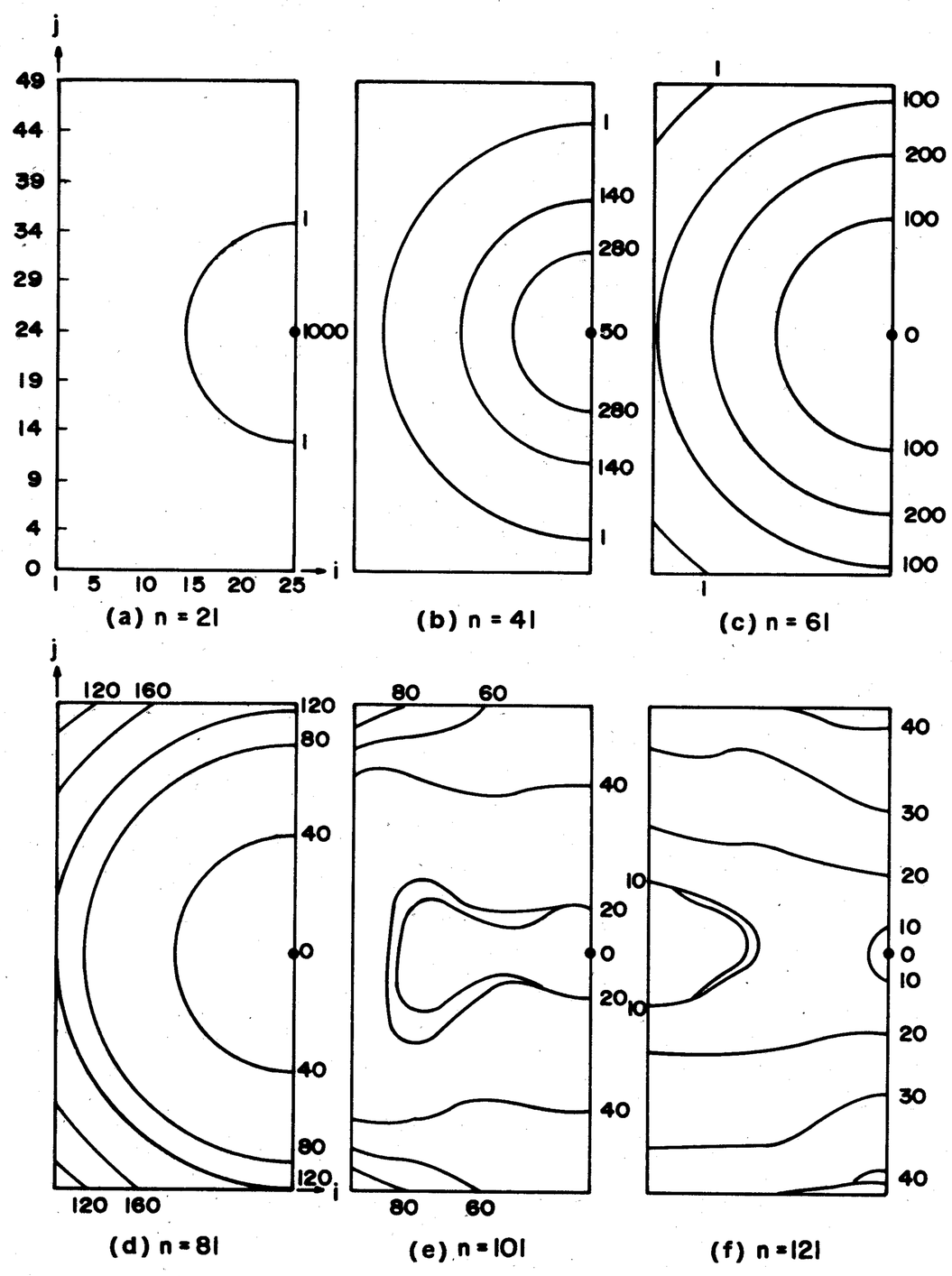

Fig. 4. Propagation of an outgoing cylindrical wave in the grid of Fig. 3.

appears to propagate off the edges of the grid, as desired, with only slight distortion of the nominal cylindrical shape. The residual field magnitude in Fig. 4(e)(f) is about one order of magnitude less than the peak outgoing fields at the grid boundaries in Fig. 4(c) (d). Further, the residual field continues to propagate off the grid. This example shows that (9a)–(9d) reduce grid-boundary reflection to the point where a first-order correct solution of continuous irradiation scattering problems is feasible.

Truncation conditions (9a)–(9d) are useful for an assumed y-directed incident plane wave, with field components E_z and H_x for scattering problems. First, (9a) and (9b) reduce to an exact truncation, similar to (8a), for such a wave. Second, (9c) and (9d) have no effect on the propagation of such a wave, which lacks an H_y component. Therefore, this lattice truncation effectively makes the lattice boundary invisible to a y-directed incident plane wave.

IV. THE PLANE-WAVE-SOURCE CONDITION

We now consider the simulation of a continuous, sinusoidal, incident plane wave for use in scattering problems. The simplest approach is to vary the electric field at all points along one endface of the lattice in a sinusoidal manner. This lattice plane would then radiate the desired plane wave. However, such a specification of field values at a lattice boundary plane, without consideration of the values of the fields of any possible outgoing scattered waves, represents a hard lattice truncation condition and would cause undesired reflections.

An example of a soft plane-wave-source condition is illustrated using the two-dimensional lattice of Fig. 3

$$E_z^n(i,2) \leftarrow 1000 \sin (2\pi f n \delta t) + E_z^n(i,2). \qquad (10)$$

Equation (10) is a modification of the Maxwell's equations algorithm for all points on the grid line $j = 2$. At each point on this line, the computer first calculates E_z^n in the normal manner of the algorithm, and stores the value in memory. Then the value of the sinusoid is calculated and added to the stored value of E_z^n. Finally, this modified value of E_z^n is stored in memory, In effect, (10) simulates the linear superposition of a y-directed plane wave and the ambient field along the grid line $j = 2$; (10) generates the desired sinusoidal, incident plane wave. But most importantly, (10) permits any scattered, outgoing wave to propagate right through the plane-wave source at $j = 2$ without reflection and reach the soft grid truncation at $j = 0$ to be absorbed. This condition simulates a plane wave originating at infinity, and a scattered wave returning to infinity, without permitting any interaction between the two waves except at the scatterer.

V. THE SYMMETRY CONDITIONS

An important savings of computer memory and program execution time results if even symmetry of the dielectric scatterer about one or two lattice planes can be assumed. An example of the programming of even scatterer symmetry is illustrated using the two-dimensional lattice of Fig. 3. The scatterer is assumed to be evenly symmetric about the grid line $i = 25\frac{1}{2}$

$$\mu,\epsilon,\sigma(25\tfrac{1}{2} + I,j) = \mu,\epsilon,\sigma(25\tfrac{1}{2} - I,j). \qquad (11a)$$

The incident radiation is assumed to be a $+y$-directed plane wave. The incident field components E_z and H_x are uniform in the x–z plane and thus naturally have even symmetry about $i = 25\frac{1}{2}$. Therefore, the E_z and H_x components of the total field must also possess even symmetry about $i = 25\frac{1}{2}$

$$E_z^n,H_x^n(25\tfrac{1}{2} + I,j) = E_z^n,H_x^n(25\tfrac{1}{2} - I,j). \qquad (11b)$$

Using the symmetry, the grid of Fig. 3 may be truncated at the line $i = 26$. The required truncation condition

$$E_z^n(26,j) = E_z^n(25,j) \qquad (12)$$

allows calculation of the complete set of field components, with full specification of the assumed symmetry of the problem.

VI. RESULTS OF TWO-DIMENSIONAL SCATTERING PROBLEMS

In this section, we shall present the computed results for the internal electric field of a uniform, circular, dielectric cylinder scatterer. The cylinder is assumed to be infinite in the z direction. The incident radiation is assumed to be a $+y$-directed TM wave of frequency 2.5 GHz. Because

there is no variation of either scatterer geometry or incident fields in the z direction, this problem may be treated as the two-dimensional scattering of the incident wave, with only E_z-, H_x-, and H_y-fields present. Thus the two-dimensional grid of Fig. 3 is used.

The geometry of the scatterer relative to the grid is illustrated in Fig. 5. The cylinder axis is chosen as the line $25\frac{1}{2},24\frac{1}{2},k$, allowing symmetry condition (12) to be used to truncate the grid at $i = 26$. Soft grid truncation conditions (9a), (9b), and (9c) are used to tuncate the grid at $j = 0$, $j = 49$, and $i = \frac{1}{2}$, respectively. Soft plane-wave-source condition (10) is used to generate the incident wave at $j = 2$. The grid coordinates internal to the cylinder, determined by

$$((i - 25\tfrac{1}{2})^2 + (j - 24\tfrac{1}{2})^2)^{1/2} \leq 20 \qquad (13)$$

are assigned the dielectric parameters ϵ_d, μ_0, and σ_d. All grid points outside of the cylinder are assigned the parameters of free space. Equation (13) leads to a stepped-edge approximation of the circular boundary of the scatterer. The program is started by setting all field components of the grid equal to zero. The plane-wave source is activated at $n = 1$, the first time step of the algorithm, and left on during the entire run. The program is time stepped to n_{max} chosen large enough so that the sinusoidal steady state is achieved.

The first cylinder scatterer program has the following parameters: $\epsilon_d = 4\epsilon_0$, $\sigma_d = 0$, $\delta = 0.3$ cm $= \lambda_d/20$, $\delta t = 5$ ps $= \delta/2c$. The choice of δ implies that the cylinder has a radius equal to λ_d. The choice of δt implies that one wave cycle requires 80 time steps of the algorithm. The computed results of this program are detailed in Fig. 6(a), which graphs the envelope of $E_z^n(25,j)$, and in Fig. 6(b), which graphs the envelope of $E_z^n(15,j)$ for $460 \leq n \leq 500 = n_{max}$. The exact solution, calculated using the summed-series technique of Jones [7], is plotted with each computed solution for comparison. The computed solution locates the positions of the peaks and nulls of the envelope of E_z^n with a maximum error of $\pm\delta$, or about ± 3 percent of the diameter of the scatterer. The computed solution gives the magnitude of the envelope at each peak with a maximum error of ± 10 percent. The execution time is 50 s using the CDC 6400.[1]

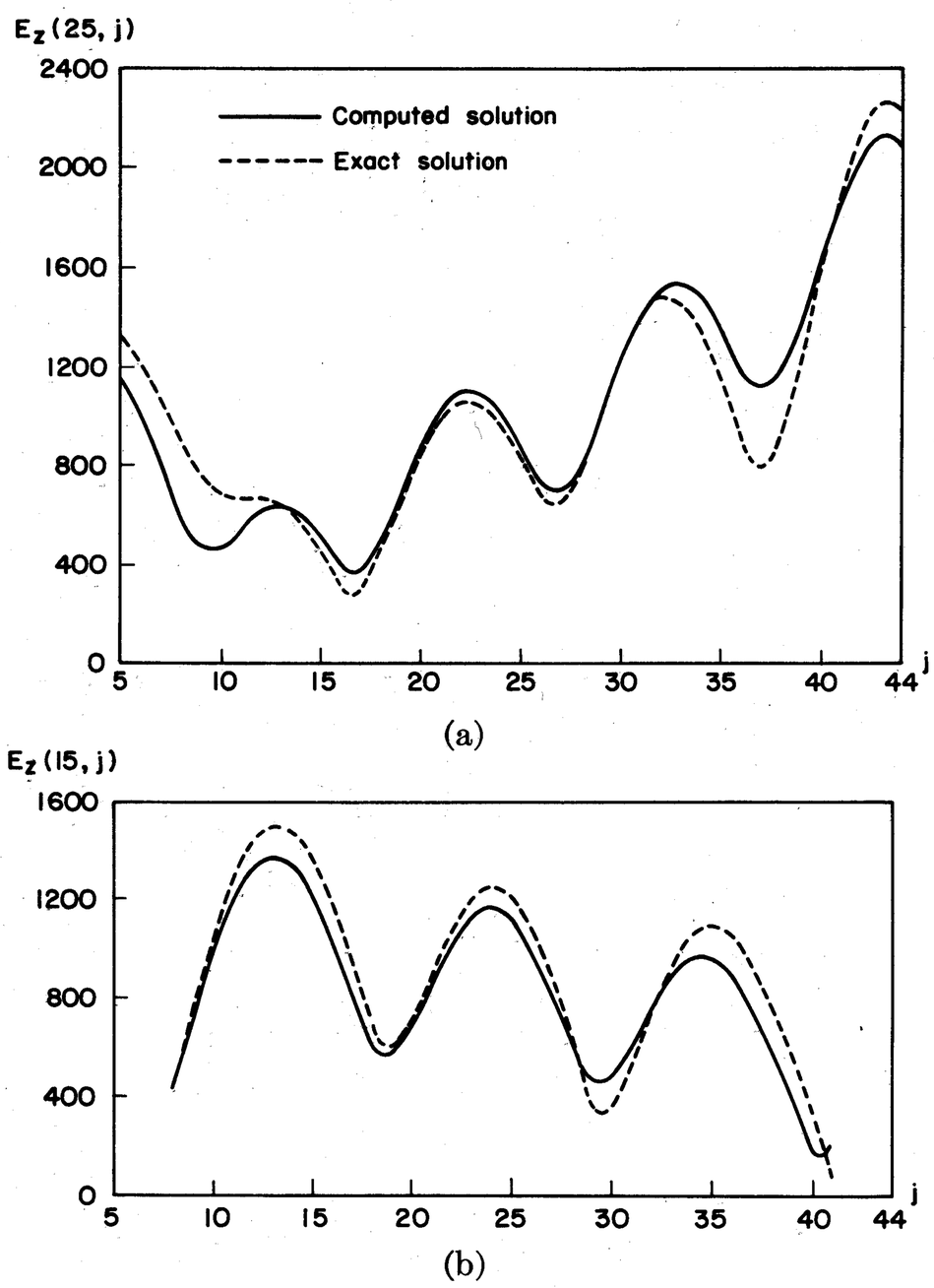

Fig. 6. Results of the first cylinder scatterer program.

The second cylinder scatterer program has the following parameters: $\epsilon_d = 47\epsilon_0$, $\sigma_d = 2.2$ mho/m, $\delta = 0.6$ mm $\approx \lambda_d/28$, $\delta t = 1$ ps $= \delta/2c$. The choice of δ implies that the cylinder has a radius equal to $\frac{2}{3}\lambda_d$. The choice of δt implies that one wave cycle requires 400 time steps of the algorithm. The dielectric parameters are chosen to simulate human tissue with high water content. The radius of the scatterer is chosen to equal that of the eyeball. The computed results of this program are detailed in Fig. 7(a), which graphs the envelope of $E_z^n(25,j)$, and in Fig. 7(b), which graphs the envelope of $E_z^n(15,j)$ for $400 \leq n \leq 600$. The exact solution is plotted with each computed solution for comparison. The computed solution locates the positions of the peaks and nulls of the envelope with a maximum error of $\pm 3\delta$, or about ± 8 percent of the diameter of the scatterer. The computed solution gives the magnitude of the central peak of the envelope with an error of ± 5 percent. The execution time is 60 s.

There are two main sources of error in the results of Figs. 6 and 7. The first is the imperfection of the soft grid truncation of (9a)–(9c). The second is the stepped-edge ap-

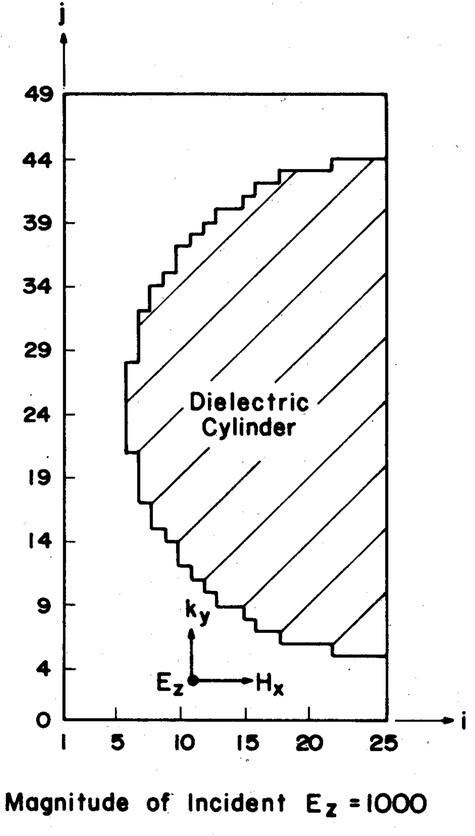

Fig. 5. Geometry of the cylindrical dielectric scatterer relative to the grid of Fig. 3.

[1] The listing of the 134-card Fortran IV source deck is available from the authors.

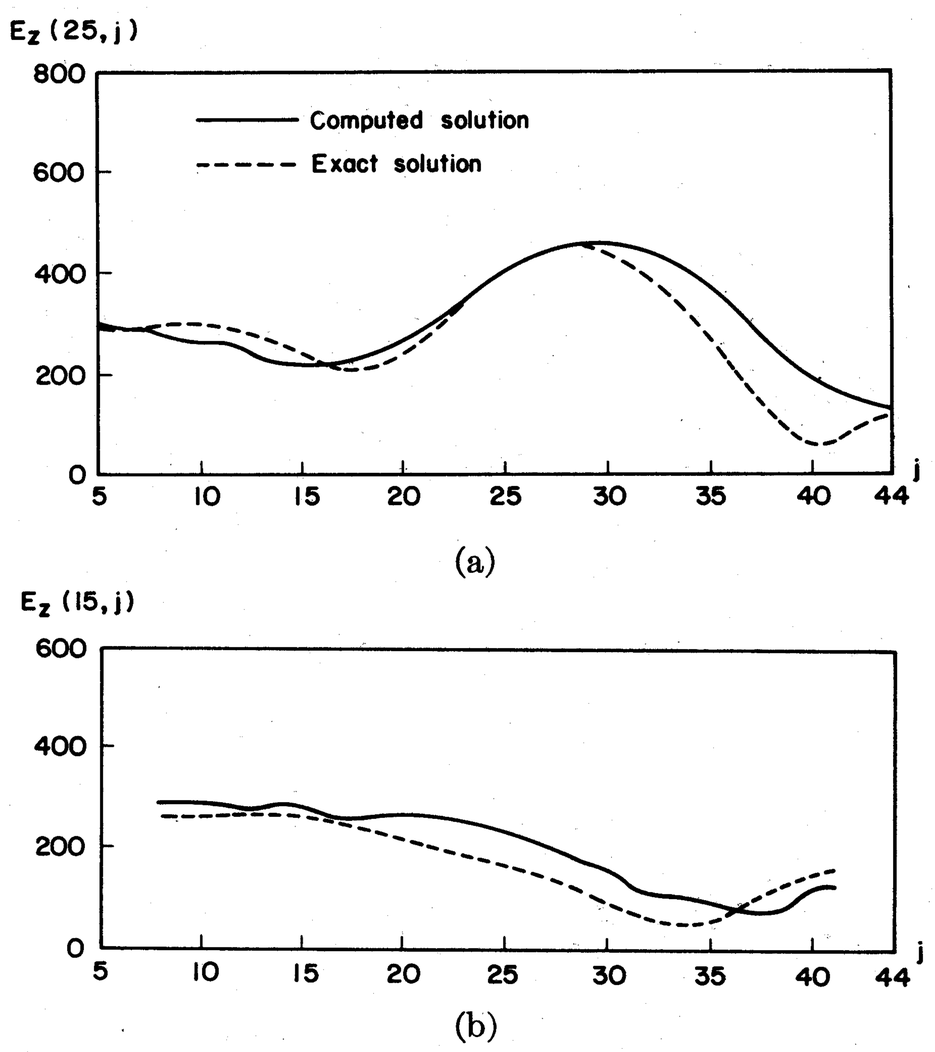

Fig. 7. Results of the second cylinder scatterer program.

proximation of the boundary of the scatterer. These error sources decrease linearly with δ, at most. Overall, the solutions of Figs. 6 and 7 may be described as better than first-order accurate. Comparable accuracy should be obtained with arbitrary two-dimensional scatterers of the general size of the cylinders examined. The only program modification required is a specification of the dielectric parameters of the arbitrary scatterer at each grid point.

VII. EXTENSION TO THREE-DIMENSIONAL SCATTERERS

The solution of three-dimensional dielectric scattering problems with this technique requires the full Yee algorithm of (6a)–(6f), in conjunction with the corresponding lattice. A sufficiently accurate lattice truncation condition, similar to (9a)–(9d), is formulated. For this case, care must be taken in setting the truncation condition to avoid algorithm instability. This may be seen by considering the application of (7) to a cubic lattice in two or three dimensions

$$\delta t \leq \frac{\delta}{c\sqrt{2}} = 0.707\delta/c \qquad \text{(2 dimensions)} \qquad (14a)$$

$$\delta t \leq \frac{\delta}{c\sqrt{3}} = 0.577\delta/c \qquad \text{(3 dimensions)}. \qquad (14b)$$

If, for convenience in programming the truncation condition, the relation $\delta t = 0.5\delta/c$ is used for both lattices, the three-dimensional lattice algorithm is closer to instability. Therefore, any perturbation of the basic algorithm with a soft lattice truncation is more likely to lead to instability in the three-dimensional case. This has been borne out by preliminary efforts in the programming of this case.

APPENDIX

DERIVATION OF THE STABILITY CRITERION

For convenience, we consider a normalized region of space with $\mu = 1$, $\epsilon = 1$, $\sigma = 0$, and $c = 1$. Letting $j = (-1)^{1/2}$, we rewrite Maxwell's equations as

$$j\nabla \times (\bar{H} + j\bar{E}) = \frac{\partial}{\partial t}(\bar{H} + j\bar{E}) \qquad (15a)$$

or more simply as

$$j\nabla \times \bar{V} = \partial\bar{V}/\partial t \quad \text{where} \quad \bar{V} = \bar{H} + j\bar{E}. \qquad (15b)$$

The stability of a particular numerical representation of (15b) can be examined simply by considering the following pair of eigenvalue problems:

$$\left.\frac{\partial}{\partial t}\right|_{\text{numerical}} \bar{V} = \lambda\bar{V} \qquad (16a)$$

$$j\nabla|_{\text{numerical}} \times \bar{V} = \lambda\bar{V}. \qquad (16b)$$

Using the numerical time derivative of (5), (16a) yields

$$\frac{\bar{V}^{n+1/2} - \bar{V}^{n-1/2}}{\delta t} = \lambda\bar{V}^n. \qquad (17)$$

Defining a solution growth factor $q = \bar{V}^{n+1/2}/\bar{V}^n$, and substituting into (17), we solve for q

$$q = \lambda\delta t/2 \pm (1 + (\lambda\delta t/2)^2)^{1/2}. \qquad (18)$$

Algorithm stability requires that $|q| \leq 1$ for all possible spatial modes in the lattice. For this to occur

$$\text{Re}\,\lambda = 0 \quad |\text{Im}\,\lambda| \leq 2/\delta t. \qquad (19)$$

We now let

$$\bar{V}(l,m,n) = \bar{V}_0 \exp\left[j(k_x l\delta x + k_y m\delta y + k_z n\delta z)\right] \qquad (20)$$

represent an arbitrary lattice spatial mode. Using the numerical space derivative formulation of (4), (16b) yields

$$-2\left[\frac{\sin(\frac{1}{2}k_x\delta x)}{\delta x}, \frac{\sin(\frac{1}{2}k_y\delta y)}{\delta y}, \frac{\sin(\frac{1}{2}k_z\delta z)}{\delta z}\right] \times \bar{V}(l,m,n) = \lambda\bar{V}(l,m,n). \qquad (21)$$

After performing the cross product and writing the x, y, and z component equations, the resulting system is solved for λ^2

$$\lambda^2 = -4\left(\frac{\sin^2(\frac{1}{2}k_x\delta x)}{\delta x^2} + \frac{\sin^2(\frac{1}{2}k_y\delta y)}{\delta y^2} + \frac{\sin^2(\frac{1}{2}k_z\delta z)}{\delta z^2}\right). \qquad (22)$$

For all possible k_x, k_y, and k_z

$$\text{Re}\,\lambda = 0 \quad |\text{Im}\,\lambda| \leq 2\left(\frac{1}{\delta x^2} + \frac{1}{\delta y^2} + \frac{1}{\delta z^2}\right)^{1/2}. \qquad (23)$$

To satisfy stability condition (19) for the arbitrary lattice

spatial mode, we set

$$2\left(\frac{1}{\delta x^2}+\frac{1}{\delta y^2}+\frac{1}{\delta z^2}\right)^{1/2} \leq \frac{2}{\delta t}. \tag{24}$$

The algorithm stability condition follows immediately from (24). In an inhomogeneous region of space, it is difficult to determine a spectrum of λ analogous to (23) for all possible lattice spatial modes. For absolute algorithm stability, (7) suffices because it represents a "worst case" choice of δt.

ACKNOWLEDGMENT

The authors wish to thank Dr. G. O. Roberts of the Engineering Sciences Department of Northwestern University for his useful comments on algorithm stability.

REFERENCES

[1] T. K. Wu and L. L. Tsai, "Numerical analysis of electromagnetic fields in biological tissues," *Proc. IEEE* (Lett.), vol. 62, pp. 1167–1168, Aug. 1974.
[2] R. F. Harrington, *Field Computation by Moment Methods.* New York: Macmillan, 1968, ch. 3.
[3] B. H. McDonald and A. Wexler, "Finite-element solution of unbounded field problems," *IEEE Trans. Microwave Theory Tech. (1972 Symp. Issue)*, vol. MTT-20, pp. 841–847, Dec. 1972.
[4] D. R. Wilton and R. Mittra, "A new numerical approach to the calculation of electromagnetic scattering properties of two-dimensional bodies of arbitrary cross section," *IEEE Trans. Antennas Propagat.*, vol. AP-20, pp. 310–317, May 1972.
[5] Vogelback Computing Center, Northwestern Univ., Evanston, Ill., Library no. NUCC288, Subroutine LUECS.
[6] K. S. Yee, "Numerical solution of initial boundary value problems involving Maxwell's equations in isotropic media," *IEEE Trans. Antennas Propagat.*, vol. AP-14, pp. 302–307, May 1966.
[7] D. S. Jones, *The Theory of Electromagnetism.* New York: Macmillan, 1964, pp. 450–452.